

# EXPERIMENTAL AND NUMERICAL INVESTIGATIONS TO EXTEND THE VALIDITY RANGE OF A TURBINE LOSS CORRELATION FOR ULTRA-LOW ASPECT RATIOS IN TRANSONIC FLOW

A. Beschorner<sup>1</sup> - K. Vogeler<sup>1</sup> – E. Goldhahn<sup>2</sup> – M. Huhnd<sup>2</sup>

<sup>1</sup> Technische Universität Dresden, Chair of Turbomachinery and Jet Propulsion, Dresden Germany, andre.beschorner@mailbox.tu-dresden.de

<sup>2</sup> Airbus, Airbus-Allee 1, Bremen Germany

## ABSTRACT

The target of the investigation presented in this paper was to develop a loss correlation for ultra-low aspect ratio turbine blades, with validity in the transonic flow regime. A set of public correlations has been used as a basis for the validity range extension. The database for the correlation development has been created by the results of 3D CFD computations. The numerical model has been validated by experimental investigations in a newly designed transonic testrig with pneumatic and optical measurement methods. The comparison between the computed and the measured cascade results showed good conformance. Finally the paper will present the necessary modifications to the complete set of correlations to meet the computed loss coefficients of the CFD database.

## NOMENCLATURE

AR	aspect ratio (h/c)	$Y_S$	secondary loss coefficient
c	chord	$Y_{S,BSM}$	secondary loss coefficient according to Benner <i>et al.</i>
$C_L$	airfoil lift coefficient, eq. 16	$Y_{TE}$	trailing edge loss coefficient
$c_x$	axial chord length	$Y_{Tc}$	tip clearance loss coefficient
$F_t$	tangential loading factor	$Y_{TcAR}$	tip clearance, aspect ratio loss
$F_{AR}$	aspect ratio influence factor	$Y_{Pba}$	Profile loss for impulse blading
g	absolute radial gap size	$Y_{Pb0}$	Profile loss for nozzle blading
h	channel height	$\alpha$	flow angle measured from axial
K	correlation factor defined in text	$\alpha_m$	mean gas angle defined in eq. 17
Ma	Mach number	$\alpha_{lim}$	pre-defined limit outlet angle
P	total pressure	$\beta$	blade metal angle measured from axial direction in degrees
p	static pressure	$\gamma$	ratio of specific heat capacities
q	dynamic head (P-p)	$\delta^*$	boundary layer displacement thickness at the trailing edge
Re	Reynolds number based on true chord and outlet velocity	$\Phi$	stagger angle measured from axial direction
S	spacing between blades (pitch)	$\Delta\Phi_{TET}$	trailing edge kinetic energy loss
$t_{max}$	maximum blade thickness	$\sigma$	blade row solidity =c/S
tet	trailing edge thickness	$\tau$	relative gap size =g/h
tw	throat width	Subscripts:	
Y	total pressure loss coefficient $\Delta P/q$ where q is taken at blade outlet	1,2	inlet, outlet
$Y_p$	profile loss coefficient		

## INTRODUCTION

Loss correlations are used for mean-line performance prediction calculations in turbomachinery design. The standard way to develop loss correlations would be to directly use experimental results. In the geometry range of ultra-low aspect ratio in combination with transonic flow these

measurements are not possible. Therefore a different way to create the database has been used.

Experimental investigations in a transonic cascade test-rig with 10mm channel height have been used to validate numerical cascade calculations which represented the same geometry. Measured physical values have been total and static pressure and total temperature at inlet and the far outlet. Moreover the complete density field has been determined using conventional schlieren and background oriented schlieren techniques. From the cascade calculations periodic CFD setups have been derived and varied to create the database for loss correlation extension. Using a validated numerical code instead of the experiment has enormous advantages in terms of flexibility, range and time in data processing. The solution accuracy of CFD is seen as high enough to be used for loss correlation extension.

With the described strategy it was possible to extend the gap free turbine loss prediction of Benner *et al.* (2006) to a range of aspect ratios below unity. In the aspect ratio range above unity the loss prediction already showed good conformance to the CFD database. Moreover the gap loss correlation of Yaras and Sjolander (1992) has been modified to correlate with the computed results in the low aspect ratio range with gap sizes of 2.5%, 5% and 7.5% channel height. A good prediction quality within an absolute difference of  $\pm 0.05$  between correlation and CFD results was reached. The modified loss correlation was implemented in a turbine design tool. Hence it is tested for usability in design calculations.

The presented paper will describe the experimental and numerical setup, the relevant loss correlations from open literature and the modifications of the correlations to extend their validity range. Important literature will be mentioned in each chapter separately.

## REVIEW ON PUBLIC TURBINE LOSS CORRELATIONS

The history of the equation set for turbine loss prediction used in this paper, started with Ainley and Mathieson (1951). With improvements in turbine technology this set of equations has been consequently updated e.g. by Dunham and Came (1970) and Kacker and Okapuu (1982). The basic principle of these loss correlations is the breakdown of the total pressure loss into several parts according to the source of loss. Recently developed improvements to this set of loss correlation refer to the single parts of the model.

Benner *et al.* (2006) defined a new superposing principle for secondary and profile loss and updated the secondary loss coefficient using a set of 34 cascade geometries. Zhu and Sjolander (2005) refined the profile loss prediction using a large database of measured profile losses including a notable number of recently developed highly loaded low pressure turbine airfoils. Improvements have been made for the Reynolds number dependency and the applicability of the profile loss for inlet guide vanes.

The comparison of different gap loss prediction models by Matsunuma (2006) showed that the correlations of Kacker and Okapuu (1982), Denton (2004) and Yaras and Sjolander (1992) predicted the measurement results well. The model of Yaras and Sjolander will be used in the current investigation because it perfectly fits into the complete set of correlations.

The following part of the paper will describe the basic equations of the here used loss prediction models. The used angle definition is conform to those of Benner *et al.* (2006) and is shown in Fig. 1. A good overview on this set of correlations and a set of polynomial equations for the graphically presented loss values of Ainley and Mathieson is given by Tournier *et al.* (2010).

### Main Model Definition

The total pressure loss coefficient is defined in equation (1). In the Benner/Sjolander loss correlation the profile loss and the secondary loss are superposed (2) using a factor for the penetration depth (3) of the secondary loss into the flow channel.

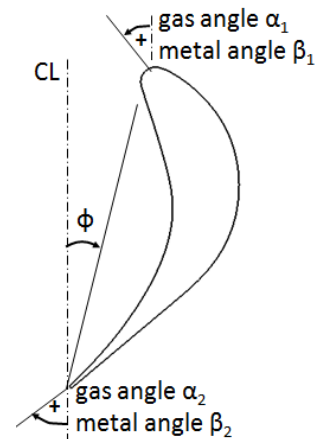


Fig. 1 Angle definition

$$Y = (Y_P + Y_S) + Y_{TE} + Y_{TC} \quad (1)$$

$$(Y_P + Y_S) = (1 - Z_{TE}/h) \cdot Y'_P + Y'_S \quad (2)$$

$$\frac{Z_{TE}}{h} = \frac{0.1 \cdot |F_t|^{0.79}}{\sqrt{\cos \alpha_1 / \cos \alpha_2} (h/c)^{0.55}} + 32.7 \left( \frac{\delta^*}{h} \right) \quad (3)$$

### Profile Loss

The profile loss coefficient used for the current investigation is based on the work of Zhu and Sjolander (2005). Compared to the profile loss definition of Kacker and Okapuu (1982), they improved the Reynolds number influence ( $K_{Re}$ ) and the validity of the model for inlet guide vanes ( $K_{in}$ ).

$$Y'_P = 0.914 \cdot [K_{in} Y'_{P,AM} K_P + Y_{shock}] \cdot K_{Re} \quad (4)$$

The Zhu/Sjolander profile loss uses a modification of the Ainley/Mathieson profile loss coefficient, which is calculated by superposing measured losses of impulse and nozzle type turbine blades.

$$Y'_{P,AM} = \left\{ Y_{Pb0} + \left| \frac{\beta_1}{\alpha_2} \right| \cdot \left( \frac{\beta_1}{\alpha_2} \right) \cdot [Y_{Pba} - Y_{Pb0}] \right\} \left( \frac{t_{max}/c}{0.2} \right)^{K_m \frac{\beta_1}{\alpha_2}} \quad (5)$$

The Reynolds number correction proposed by Zhu is calculated as:

$$K_{Re} = \begin{cases} \left( \frac{2 \times 10^5}{Re} \right)^{0.575} & \text{for } Re < 2 \times 10^5 \\ 1.0 & \text{for } Re \geq 2 \times 10^5 \end{cases} \quad (6)$$

In the paper of Ainley and Mathieson (1951) it is mentioned that the value of  $t_{max}/c$  should be restricted to the range between 0.15 and 0.25. If the geometry is out of the given range the limit value should be taken for the computation.

The computation of the parameters in this main equation is described in detail in the paper of Tournier *et al.* (2010). In this article they also give polynomial equations for the graphically given loss values  $Y_{Pba}$  and  $Y_{Pb0}$  of Ainley and Mathieson (1951).

### Secondary Loss Coefficient

The secondary loss correlation is given by Benner *et al.* (2006) in part II. The main equation for the secondary loss coefficient is the following:

$$Y_{S,BSM} = F_{AR} \cdot \frac{0.038 + 0.41 \cdot \tanh \left( 1.2 \frac{\delta^*}{h} \right)}{\sqrt{\cos \Phi} \cdot \left( \frac{\cos \alpha_1}{\cos \alpha_2} \right) \cdot \left( \frac{c \cos \alpha_2}{c_x} \right)^{0.55}} \quad (7)$$

The factor for the aspect ratio has two different definitions depending on the blade aspect ratio of the current geometry.

$$F_{AR} = \begin{cases} AR^{-0.55} & , \text{if } AR \leq 2 \\ 1.36604 \cdot AR^{-1} & , \text{if } AR > 2 \end{cases} \quad (8)$$

For the development of this new secondary loss correlation Benner *et al.* used cascade geometries with axial aspect ratios between 1.006 and 3.833. Hence blades with aspect ratios below unity are not valid in the current model.

### Trailing Edge Loss Coefficient

$$\Delta\phi_{TE} = \Delta\phi_{b0} + \left| \frac{\beta_1}{\alpha_2} \right| \cdot \left( \frac{\beta_1}{\alpha_2} \right) \cdot [\Delta\phi_{ba} - \Delta\phi_{b0}] \quad (9)$$

The definition for the trailing edge kinetic energy loss coefficient is given by Kacker and Okapuu (1982) as presented in equation (9). The trailing edge losses depend on the trailing edge thickness, the throat width, in- and outlet angle, Mach number and specific heat ratio.

The polynomial functions for the trailing edge energy coefficients for impulse and nozzle blading ( $\Delta\phi_{ba}$  and  $\Delta\phi_{b0}$ ) are given by Tournier *et al.* (2010). Unfortunately these functions will produce negative solutions for very small relative trailing edge thickness values, which is physically not correct. Therefore modifications are necessary which are described in the last part of this paper. The original polynomial equations are the following:

$$\Delta\phi_{b0} = 0.59563 \cdot \left( \frac{tet}{tw} \right)^2 + 0.12264 \cdot \left( \frac{tet}{tw} \right) - 2.2796 \times 10^{-3} \quad (10)$$

$$\Delta\phi_{ba} = 0.31066 \cdot \left( \frac{tet}{tw} \right)^2 + 0.065617 \cdot \left( \frac{tet}{tw} \right) - 1.4318 \times 10^{-3} \quad (11)$$

The conversion of the trailing edge kinetic energy loss coefficient into the pressure loss coefficient is given by

$$Y_{TE} = \frac{\left\{ 1 - \frac{\gamma-1}{2} Ma_2^2 \cdot \left( \frac{1}{1 - \Delta\phi_{TE}} - 1 \right) \right\}^{-\gamma/(\gamma-1)} - 1}{1 - \left( 1 + \frac{\gamma-1}{2} Ma_2^2 \right)^{-\gamma/(\gamma-1)}} \quad (12)$$

### Gap Loss Prediction model

The model used for tip-leakage loss prediction is the one of Yaras and Sjolander (2006). The model is defined by the following equations.

$$Y_{TC} = Y_{tip} + Y_{gap} \quad (13)$$

$$Y_{tip} = 1.4K_E\tau \cdot \frac{\cos^2 \alpha_2}{\cos^2 \alpha_m} \cdot C_L^{1.5} \quad (14)$$

$$Y_{gap} = 0.0049K_G\sigma \cdot \frac{c}{h} \cdot \frac{\sqrt{C_L}}{\cos \alpha_m} \quad (15)$$

For mid loaded blades the coefficients  $K_E$  and  $K_G$  will be 0.5 and 1.0 respectively. For front- and aft-loaded blades  $K_E = 0.566$  and  $K_G = 0.943$ . The theoretical blade lift coefficient can be calculated with the following equation which is given by Tournier *et al.* (2010).

$$C_L = \frac{2}{\sigma} \cdot \cos \alpha_m \cdot [\tan \alpha_1 + \tan \alpha_2] \quad (16)$$

$$\alpha_m = \tan^{-1}[0.5(\tan \alpha_1 - \tan \alpha_2)] \quad (17)$$

Regarding the suggested application range of the here described loss models it can be highlighted, that for example the secondary loss model is explicitly limited to turbines where the secondary flow effects are not merged which is not true for very low aspect ratios. An exact limit value is not given by Benner *et al.* (2006).

### EXPERIMENTAL SETUP

Experimental investigations to capture the influence of the aspect ratio on the turbine losses have been performed by Ohlsson (1964), Rogo (1968) and Mobarak *et al.* (1985). In the work of

Mobarak four gap free cascade geometries with aspect ratios of 0.654, 0.545, 0.327 and 0.145 have been investigated. The blade chord length was 55mm, the flow turning  $85^\circ$  and the maximum outlet Mach number 0.6. For the channel heights of 36 and 30mm the secondary flow effects could be found in the typical form of two separate loss cores in the cascade wake. For the small flow channels with 18 and 8mm height these two loss cores were found to be merged to a single loss core with even higher effect on the overall pressure loss. The same effect could be found within the CFD results in the current work.

It was already mentioned by Ainley and Mathieson (1951) that it is not only the aspect ratio but the channel height that influences the kind of secondary loss. Benner *et al.* (2006) consciously precluded low aspect ratio geometries where secondary loss cores are most likely to be merged from the database for their loss model.

The measurements to validate the numerical model have been performed in a newly designed transonic testrig. The experimental setup in the Dresden Turbomachinery test laboratory is shown in Fig. 2. The pressurized air is coming from a tank which is fed by a screw compressor.

Conical total pressure probes of 3mm diameter are installed at MP1 and MP2, where MP2 is 7.3 chord lengths downstream the center blade. The Reason to choose a for field measurement plane is the setup of the testrig with a very low channel height combined with transonic flow. A measurement close to the cascade exit plane would have enormous effects on the cascade flow due to shocks and flow obstruction. The probes can be automatically traversed in tangential direction. Static pressure tapings are distributed directly in front of the cascade, at MP2 and at the upper and lower tailboard. The density field in the near area of the cascade can be observed with a conventional schlieren system. The mirrors of the system have a diameter of 250mm, which limits the observation area. The complete cascade wake can be observed with a background oriented schlieren system, using a dot pattern, a PIV camera and PIV evaluation software.

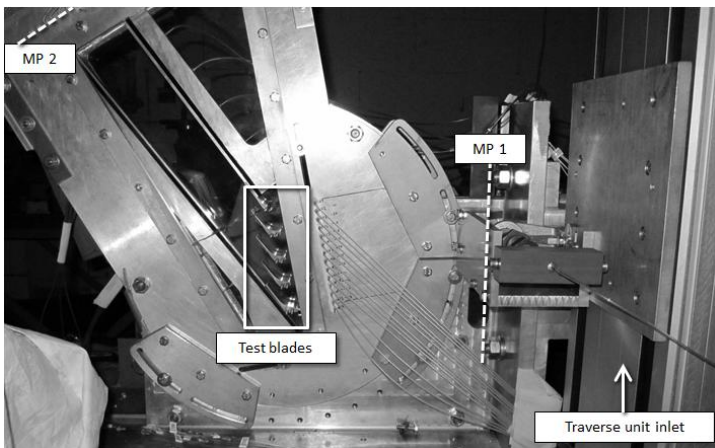


Fig. 2 Turbine cascade testrig for transonic flow (in incidence test configuration)

With modifications, the testrig also enables for incidence tests and channel height variation. Four different spline based blades have been tested. The main geometry facts are shown in Fig. 3. Blade 1 and 2 have the same flow turning but blade 2 is a Laval-type blade. Blade 3 and 4 are derived from blade 1 but with higher flow turning. A sketch of the airfoils for blade 1 and 2 is shown in Fig. 3. In the testrig there are 3 blades in the free stream and 2 blades forming the upper and lower sidewall.

	BL1	BL2	BL3	BL4
Flow turning [°]	62.5	62.5	90	105
inlet flow angle $\alpha_1$ [°]	0	0	20	25
Chord length [mm]	44.3	43.3	44.3	44.3
aspect ratio	0.226	0.231	0.226	0.226
min. distance one section [mm]	12.58	12.48	12.58	10.35
Throat four sections [mm <sup>2</sup> ]	503.31	499.28	503.09	413.90




Fig. 3 Blade and cascade attributes and sketch of blade 1 and blade 2 (Laval-type)

## VALIDATION OF NUMERICAL MODEL

The real testrig cascade geometry has been rebuilt with a structured 3D mesh to verify the numerical setup. The mesh around the blades is built by a O4H-topology. The whole cascade mesh consists of 8.3 Million cells. The geometry has a channel height of 10mm, an inflow section of 200mm and an outlet section of 354mm downstream the uppermost blade which equals 8 times the chord length. In this way the measurement planes of the original channel are included in the mesh geometry. Hence the flow characteristics can be compared at the same position. For the simulation and the mesh generation the software package Fine™/Turbo has been used. The used turbulence model for all computations is Spalart Allmaras.

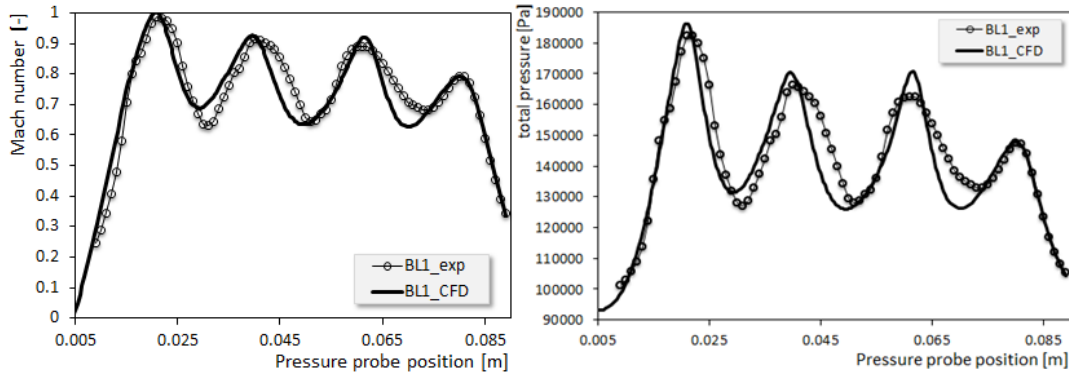


Fig. 4 Mach number and total pressure at MP2 for BL1 at the operation point of 2bar inlet pressure

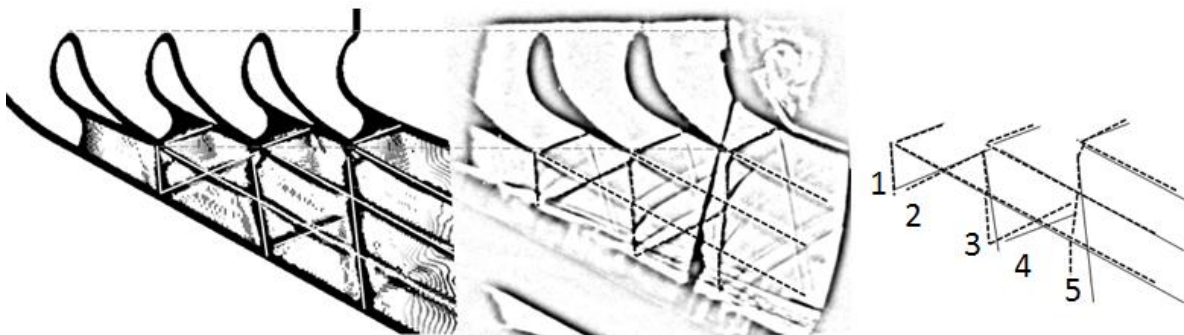


Fig. 5 Density field in the near cascade wake CFD (left), experiment (middle) and comparison

Figure 4 compares the total pressure and Mach number in the far outlet measurement plane (MP2) in 50% channel height position for CFD and experiment at the operation point of 2bar inlet pressure. The CFD gives reasonably good agreement with measurement results.

The density field near the blades is compared in Fig. 5. It shows that the CFD computation predicts the oblique shocks near the blades well. Even the shock reflections from the tailboard are shown by the numerical solution.

A detailed comparison of the shock angles is shown in Fig. 5 on the right side. The used lines for the angle comparison are also shown in the CFD solution and in the schlieren picture as well with white and black dashed lines respectively. The first shock (1) which is induced by the trailing edge of the left blade shows the same angle in the testrig and the CFD solution. The angle of the reflected shock (2) is predicted slightly lower by the CFD. Shock number three must be evaluated in two parts. The first part near the blade trailing edge shows conformity between measured and computed solution. The schlieren picture shows that shock three becomes perpendicular to the flow direction while passing the blade wake. This effect is not shown by the numerical results. Due to the different impingement angle between tailboard and shock three, the reflected shock (4) is also not conform. The description of (3) also applies for (5).

In the schlieren photograph there is a shock like line passing the whole flow field downstream of the cascade. This shadow is caused by a crack in the glass sidewall. Moreover the schlieren

picture shows lines near the lower tailboard with a  $5^\circ$  angle to it. These shadows are caused by ‘fingerprints’ of the tailboard rubber seal and its different positions during the measurement campaign.

The final straight shock behind the cascade can only be detected with the background schlieren technique since the necessary observation area is too large for the conventional schlieren system. Comparing the position of this shock in experiment and CFD shows that its distance behind the trailing edge of the uppermost blade is the same.

A flow separation on the left sidewall which is caused by the straight shock impingement is visible in the pressure chart (Fig. 4) and in the Mach number visualization (Fig. 6) as well. This separation is predicted by the numerical model as it was measured in the cascade testrig.

Summarizing all the comparisons it can be concluded that the used CFD model is capable of predicting reasonable flow results for the used geometry and flow regime. To reduce the computational effort in the geometry variation the plane cascade has been approximated by periodic, annular, non-rotating geometries with a hub radius of 1.023m, hence each passage is close to a plane cascade (the hub to tip ratio for the configuration with  $h=10\text{mm}$  is 0.99). In the periodic meshes the same O4H mesh configuration as in the plane cascade setup has been used.

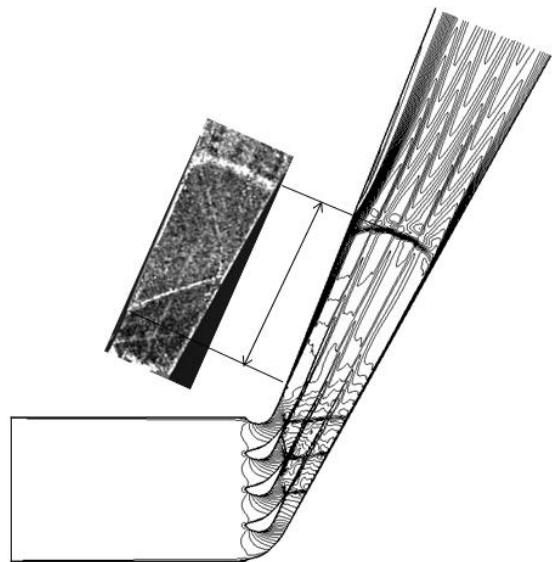


Fig. 6 **Background oriented Schlieren and CFD Mach number in the cascade wake**

## CFD DATABASE FOR CORRELATION DEVELOPMENT

The current investigation is not the first time CFD has been used to increase the validity range of a loss correlation. In the work of Javed *et al.* (2010) the loss model for a radial compressor has been improved. The extended loss correlation showed good conformance to measured results. Horlock and Denton (2005) analyzed the prediction quality of CFD for special phenomena in a typical turbomachinery flow. They concluded that the prediction quality of effects like gap flow and secondary flow is in an acceptable range.

In the current investigation a database of 34 geometry variants has been used to extend the validity range of the above presented set of loss prediction equations. To build up the database blade 4 has not been used due to flow separations on the suction side in the experimental and numerical results. Blade 1 and 2 are similar regarding their geometry parameters for the loss model. Hence only blade 1 and a modification of blade 3 with increased chord (53.3mm) have been used to create the database.

Channel heights of 4, 5, 6, 7, 8, 10, 15, 20, 25, 35, 53, and 80mm have been used for geometry variation. Hence the aspect ratio varies between 0.075 and 1.5. To capture the tip clearance influence different gap sizes of 0%, 2.5%, 5% and 7.5% have been created. For the tip clearance simulations the shroud is rotating ( $1000\text{rpm} \approx 110\text{m/s}$ ) to respect the effects of velocity difference between blade tip and shroud wall. The meshes with shroud gap have been directly derived from the gap free geometries. The configuration with tip gap has not been explicitly validated by the comparison of cascade computations and testrig measurements since the testrig could not include all features for a complete modeling of the desired flow physics (moving endwall). Except the increased node density in the shroud gap area, the numerical setup for the configurations with and w/o gap is similar. The resulting congruence between correlation and CFD for the high aspect ratio geometries for both geometry variants (with and w/o gap) let us conclude that it has not been an error to include tip clearance losses into the investigation.

All geometries are computed using the same boundary conditions with an inlet total pressure of



2.2bar and an outlet static pressure of 1.013bar. This leads to inlet Mach numbers of about 0.23 and outlet Mach numbers around unity. The resulting mass flow differs according to the channel size.

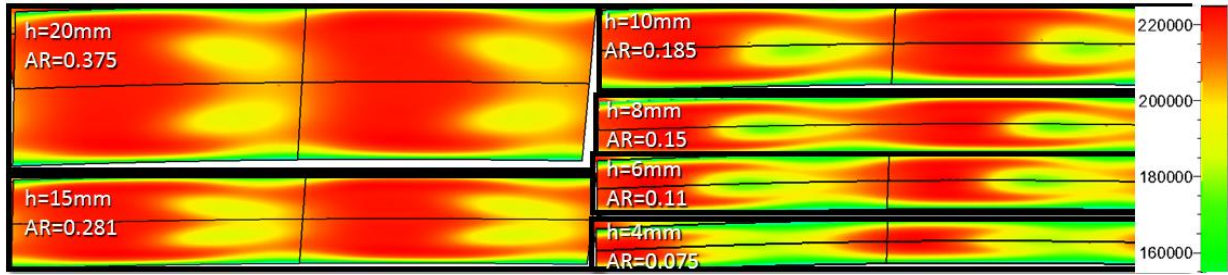


Fig. 7 Numerically computed outlet P [Pa] distributions for two passages at six different AR

Fig. 7 shows the influence of the aspect ratio on the type of secondary flow in the blade wake. Below a channel height of 10mm which equals an aspect ratio of 0.187 the secondary loss cores are merged to a single loss core which is clearly indicated by the total pressure distribution at the outlet plane. By lowering the channel height even more, the area of low pressure (light grey) increases heavily. This effect goes conform to the findings for the total pressure loss coefficient (Fig. 9), which is strongly increasing for aspect ratios below 0.2 where the merging of both secondary flow loss cores starts to happen.

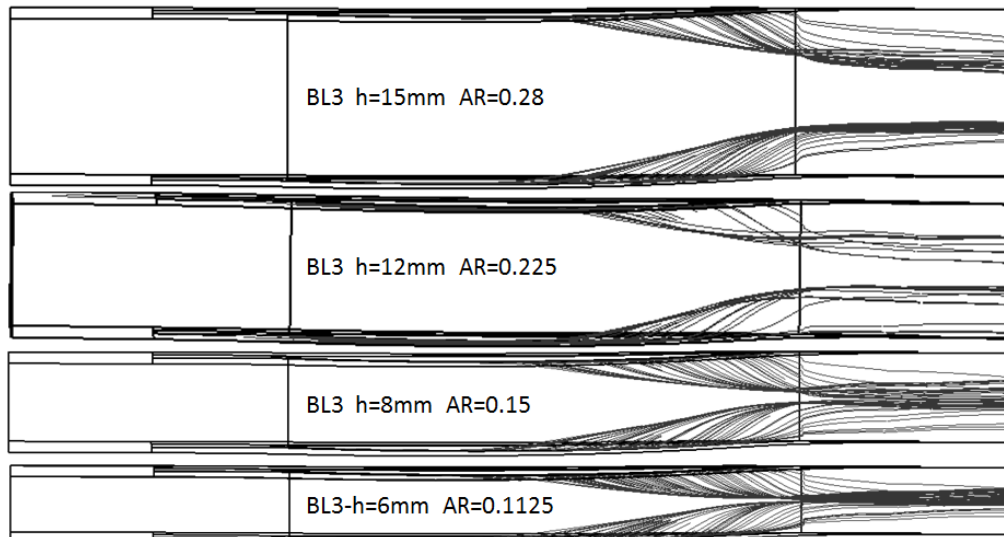


Fig. 8 Computed streamlines starting at endwall boundary layer forming the secondary flow on blade surfaces and downstream for different aspect ratios

The streamlines forming the secondary loss cores are shown in Fig. 8. Due to the pitchwise pressure gradient those streamlines starting in the endwall boundary layers are directed to the blade suction side. At about half the axial chord length the flow penetrates the blade boundary layer and moves away from the endwalls. While decreasing the aspect ratio, the percentage of spanwise penetration depth of the secondary flow rises. For channel heights below 10mm both endwall losses merge at midplane.

The loss development of the blades without gap as function of aspect ratio is shown on the left side of Fig. 9. The vertical dashed line marks the experimentally validated geometry size.

Comparing the loss correlation with the CFD computed values, a low divergence is visible for aspect ratios above unity, but an increasing deviation for aspect ratios below 0.75 is observed. This deviation is highlighted in the right chart, where the loss values are plotted as function of  $1/h$ . Moreover this chart indicates significant higher losses for the geometries with shroud gap. For high aspect ratios the tip gap configurations also show a good conformance between loss correlation and CFD, but not for the low aspect ratio configurations. The correlation for tip gap geometries is not shown in the chart, but its prediction quality can be observed in Fig. 11.



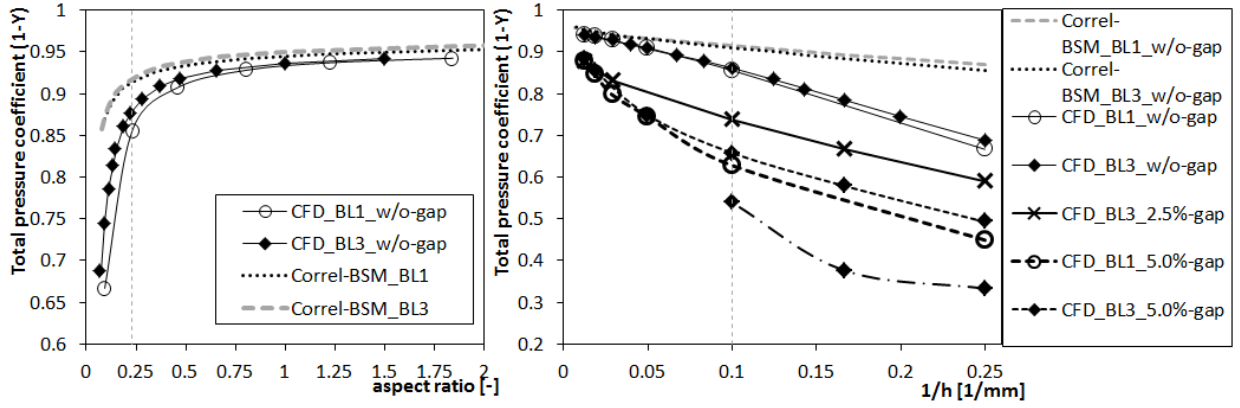


Fig. 9 Computed and predicted losses for blade 1 and blade 3 as function of aspect ratio (left) and 1/channel height (right)

### THE MODIFIED LOSS CORRELATION

The presented modifications to the loss model are necessary to include the predictability for geometries with extreme low aspect ratio including different gap sizes and to allow geometries where outlet flow angle is below the inlet angle (exhaust guide vanes).

#### Modification to the Profile Loss

In several parts of the loss model there is an interpolation between nozzle and impulse blading using the current in- and outflow angles. In the seldom case where the outflow angle is much smaller than the inlet angle and especially in the extreme case where the outlet angle is zero (EGV), the standard formulation (Equation 5) is leading to an unrealistic or no solution. The profile loss curves for different inlet angles show inflection points for an outlet angle of  $20^\circ$ . Below this angle the curves have a strong gradient and give negative loss values for outlet angles below  $\sim 11^\circ$  (depending on the inlet angle).

For the modification a limiting angle  $\alpha_{lim}$  will be implemented. Below this limit angle the computed loss will be independent of the blades outlet angle. It is suggested to select  $\alpha_{lim}$  between  $20^\circ$  and  $30^\circ$ .

$$Y'_{P,AM} = \begin{cases} \left\{ Y_{Pb0} + \left| \frac{\beta_1}{\alpha_2} \right| \cdot \left( \frac{\beta_1}{\alpha_2} \right) \cdot [Y_{Pba} - Y_{Pb0}] \right\} \left( \frac{t_{max}/c}{0.2} \right)^{K_m \frac{\beta_1}{\alpha_2}} & , if \ \alpha_2 > \alpha_{lim} \\ \left\{ Y_{Pb0} + \left| \frac{\beta_1}{\alpha_{lim}} \right| \cdot \left( \frac{\beta_1}{\alpha_{lim}} \right) \cdot [Y_{Pba} - Y_{Pb0}] \right\} \left( \frac{t_{max}/c}{0.2} \right)^{K_m \frac{\beta_1}{\alpha_{lim}}} & , if \ \alpha_2 < \alpha_{lim} \end{cases} \quad (18)$$

#### Modification to the Secondary Loss

The modification in the secondary loss model, will only affect geometries with aspect ratios below unity. The change compared to the secondary loss correlation of Benner *et al.* (2006) accounts for the aspect ratio influence factor. Its new definition is shown in the following equation:

$$F_{AR} = \begin{cases} AR^{-0.93} & , if \ AR < 1 \\ AR^{-0.55} & , if \ 1 \leq AR \leq 2 \\ 1.36604 \cdot AR^{-1} & , if \ AR > 2 \end{cases} \quad (19)$$

#### Modifications to the Trailing Edge Loss Coefficient

The polynomial equations for the trailing edge loss correlation given by Tournier *et al.* (2010) had to be modified since the results showed negative values with low trailing edge to throat ratios. These equations for nozzle and impulse blading are changed to the following ones:

$$\Delta\phi_{b0} = 0.639127 \cdot \left(\frac{tet}{tw}\right)^2 + 0.10075 \cdot \left(\frac{tet}{tw}\right) \quad (20)$$

$$\Delta\phi_{ba} = 0.338011 \cdot \left(\frac{tet}{tw}\right)^2 + 0.0518529 \cdot \left(\frac{tet}{tw}\right) \quad (21)$$

The second modification to the trailing edge loss concerns its main equation, which performs the interpolation between nozzle and impulse blading. This original interpolation equation (9) gives negative loss values if the outlet flow angle is much lower than the inlet angle, which is true for exhaust guide vanes. Hence it is necessary to modify the equations to achieve sensible solutions for the loss coefficient also for the EGV. The modified equation is shown in equation (22). It becomes valid if the outlet flow angle is below the inlet angle. In this case it is assumed that the loss equals the values for impulse blading which is the lower loss for the interpolation.

$$\Delta\phi_{TE} = \begin{cases} \Delta\phi_{b0} + \left|\frac{\beta_1}{\alpha_2}\right| \cdot \left(\frac{\beta_1}{\alpha_2}\right) \cdot [\Delta\phi_{ba} - \Delta\phi_{b0}] , & \text{if } \alpha_2 > \beta_1 \\ \Delta\phi_{ba} & , \text{if } \alpha_2 < \beta_1 \end{cases} \quad (22)$$

This second modification to the trailing edge loss coefficient is only necessary if the loss model should be used for the complete geometry range of a turbine including the EGV.

### Modifications to gap loss prediction

The original basic equation of the Yaras/Sjolander clearance loss prediction model is shown in equation (13). In order to meet the CFD computed losses for the investigated low aspect ratio geometries it was necessary to introduce an additional coefficient to the model. The computation of  $Y_{tip}$  and  $Y_{gap}$  keeps valid but the influence to the total clearance loss is decreased to 60% as given in equation (23).

$$Y_{TC} = 0.5Y_{tip} + 0.1Y_{gap} + Y_{TCAR} \quad (23)$$

The additional summand has been identified by separating the single loss elements and subtraction from the complete CFD computed loss (as shown in equation 24). The solution has been plotted for each geometry realization (Fig. 10 left) in order to create a fitting function for the new coefficient.

$$Y_{TCAR} = Y_{CFD\_w\_gap} - Y_{CFD\_w/o\_gap} - 0.5Y_{tip} - 0.1Y_{gap} \quad (24)$$

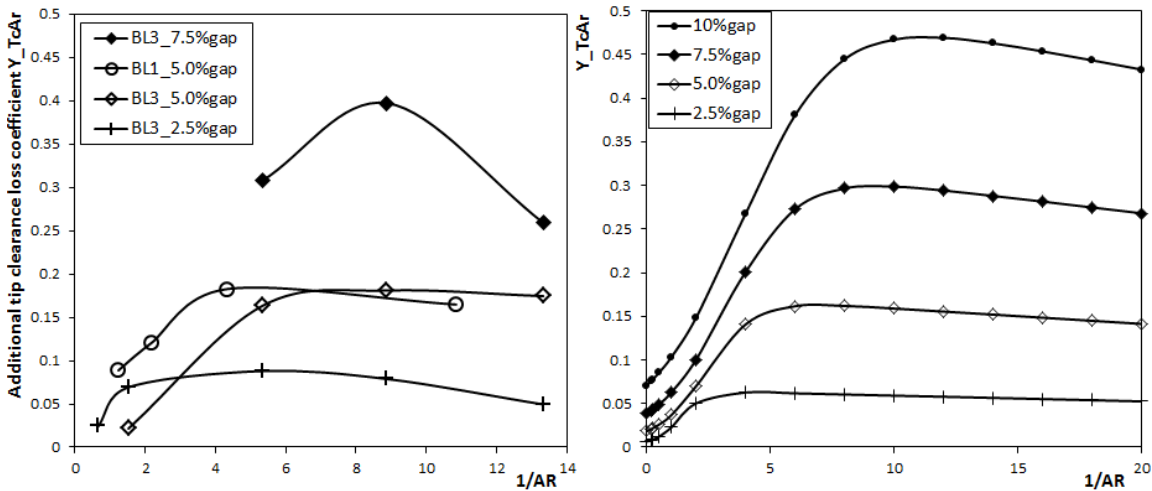


Fig. 10 Plots for the new tip clearance aspect ratio loss coefficient; left: CFD results; right: correlated results

The new summand presented in equation (25) is computed using the relative gap size  $\tau = g/h$  and the aspect ratio of the blade row. Calculated  $Y_{TcAr}$  values for different aspect ratios and relative gap sizes are shown in Fig. 10 (right) to illustrate the behavior of the additional coefficient.

$$Y_{TcAr} = \left[ \frac{38\tau^2 + 1.49\tau + 0.0022}{1 + 17.986 \cdot \exp\{-8.4\tau - 0.0576 \cdot \tau^{0.955} \cdot c/h\}} + 0.1\tau \right] \cdot \left(1 - 0.01 \frac{c}{h}\right) \quad (25)$$

### Prediction quality of the modified loss model

With the presented modifications of the loss correlation it was possible to increase its validity range to an aspect ratio of 0.2, which is represented by the geometry of the experimental validation. The used CFD database goes even further down to an aspect ratio of 0.075. For most of the tested geometries the original set of loss correlation is not valid since the aspect ratio is below unity. Nevertheless Fig. 11 compares the predictions of the original model to those of the modified model in relation to the CFD results. In the left chart the data points which are out of the validity range of the original correlation are gray colored besides the black data points which have an aspect ratio above unity. It is visible that the original loss correlation shows a good conformance to the CFD database as long as the aspect ratio is above or close to unity, which is also true for the geometries including a tip gap. For extreme low aspect ratios, far beyond the validity of the original model its predictions show a strong difference to the CFD database.

Using the modified loss correlation the prediction quality for the complete set of tested geometries is within the range of  $\pm 0.05$ . With the original set of equations the maximum prediction error is 0.2.

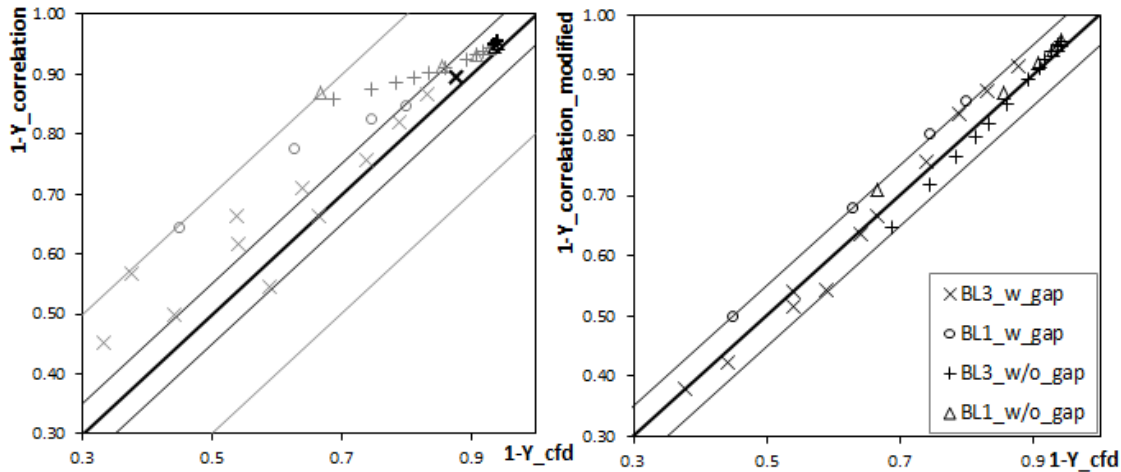


Fig. 11 Prediction quality for original set of loss equations (left) and modified loss model

## CONCLUSIONS

Based on a literature research on turbine loss correlations, numerous 3D-CFD computations with geometry variation and the measurements to validate the CFD model for a specific geometry variant, it was possible to enlarge the validity range of a loss correlation. The presented modifications to the model, enables the loss prediction for geometries with aspect ratios down to 0.2 due to the experimental validation at this point. The validity includes transonic flow.

For high aspect ratios the original set of loss correlations already reflects the CFD results of the test database. For the gap free loss model, geometries with an aspect ratio above unity are completely unaffected by the suggested modifications. For the gap loss model the suggested modifications have a marginal effect at higher aspect ratios.

Future work on the presented topic will deliver a wider range of experimental and numerical results, which enables for intensive testing on the presented correlations and modifications if necessary.

## ACKNOWLEDGEMENTS

The authors gratefully acknowledge the financial support of Airbus S.A.S..

## REFERENCES

- Ainley, D.G., and Mathieson, G.C.R., (1951) "*A method of performance estimation for axial-flow turbines*", British Aeronautical Research Council, Reports and Memoranda No. 2974.
- Benner, M.W., Sjolander, S.A., and Moustapha, S.H., (2006) "*An empirical prediction method for secondary losses in turbines – Part I: A new loss breakdown scheme and penetration depth correlation*", ASME Journal of Turbomachinery, Vol. 128, pp. 273-280.
- Benner, M.W., Sjolander, S.A., and Moustapha, S.H., (2006) "*An empirical prediction method for secondary losses in turbines – Part II: A new secondary loss correlation*", ASME Journal of Turbomachinery, Vol. 128, pp. 281-291.
- Denton, J.D., (2004) "*Axial turbine aerodynamic design*", Cambridge Turbomachinery course, Whittle Laboratory, University of Cambridge.
- Dunham, J. and Came, P.M., (1970) "*Improvements to the Ainley/Mathieson method of turbine performance prediction*", ASME Journal of Engineering for Power, A92, pp. 252-256.
- Horlock, J.H., and Denton J.D., (2005) "*A review of some early design practice using computational fluid dynamics and a current perspective*", ASME Journal of Turbomachinery, Vol. 127, pp. 5-13.
- Javed, A., Olivero, M., and Buijtenen J.P., (2010) "*Development of 1D performance analysis tool for a microturbine radial compressor using CFD*", European Conference on Computational Fluid Dynamics, Lisbon, Portugal, 14-17 June 2010.
- Kacker, S.C., and Okapuu, U. (1982) "*A mean line prediction method for axial flow turbine efficiency*", ASME Journal of Engineering for Power, 104, pp. 111-119.
- Mobarak, A., Khalafallah, M.G. and Lotayef, M., (1985) "*Effect of aspect ratio on energy loss in nozzle blades of small power turbines*", International Journal of Turbo and Jet Engines 2, pp. 299-305.
- Ohlsson, G.O., (1964) "*Low aspect ratio turbines*", Journal of Engineering for Power, pp. 13-16.
- Rogo, C., (1968) "*Experimental aspect ratio and tip clearance investigation on small turbines*", SAE PaperNo. 680448.
- Tournier, J.M., Mohamed, S., El-Genk, (2010) "*Axial flow, multi-stage turbine and compressor models*" Energy Conversion and Management, Volume 51, Issue 1, January 2010, Pages 16-29.
- Yaras, M.I., and Sjolander, S.A., (1992) "*Prediction of tip-leakage losses in axial turbines*", ASME Journal of Turbomachinery, Vol. 114, pp. 204-210.
- Zhu, J. and Sjolander, S.A., (2005) "*Improved profile loss and deviation correlations for axial turbine blade rows*", in proceedings of GT2005 ASME turbo expo 2005: power for land, sea and air, June 6-9, 2005, Reno-Tahoe, Nevada, USA, American Society of Mechanical Engineers, New York, NY, Paper No. GT2005-69077 p. 783-792.